

Criticality of the excess energy cost due to the unit-flux-quantum external field for the $(2 + 1)$ D superfluid-insulator transition

Yoshihiro Nishiyama

Department of Physics, Faculty of Science, Okayama University, Okayama 700-8530, Japan

Abstract.

The two-dimensional (2D) spin- $S = 1$ XY model was investigated numerically as a realization of the $(2 + 1)$ D superfluid-Mott-insulator (SF-MI) transition. The interaction parameters are extended so as to suppress corrections to finite-size scaling. Thereby, the external field of a unit flux quantum ($\Phi = 2\pi$) is applied to the 2D cluster by incorporating the phase factor $e^{i\phi_{ij}}$ (ϕ_{ij} : gauge angle between the i and j sites) into the hopping amplitudes. Taking the advantage in that the exact-diagonalization method allows us to treat such a complex-valued matrix element, we evaluated the excess energy cost $\Delta E(2\pi)$ due to the magnetic flux $\Phi = 2\pi$ explicitly in the SF (XY) phase. As a result, we found that the amplitude ratio $\rho_s/\Delta E(2\pi)$ (ρ_s : spin stiffness) makes sense in proximity to the critical point, exhibiting a notable plateau in the SF-phase side. The plateau height is estimated, and compared to the related studies.

1. Introduction

In two spatial dimensions (2D), the dynamical conductivity $\sigma(\omega)$ becomes a dimensionless (scale invariant) quantity [1, 2], and its Drude weight such as the spin stiffness (helicity modulus) ρ_s has the same scaling dimension as that of the elementary-excitation masses, *e.g.*, Mott-insulator (Δ) and Higgs (m_H) gaps. Hence, the critical amplitude ratio between these quantities should exhibit a universal behavior around the superfluid-Mott-insulator phase transition. Actually, as for the $(2 + 1)$ D boson system, a variety of critical amplitude ratios such as $\rho_s/\Delta = 0.414$ [3] and $m_H/\Delta = 2.2$ [4] were calculated via the renormalization-group [3, 4, 5, 6, 7] and numerical [8, 9, 10, 11, 12, 13, 14] methods; see Sec. 4.1 of Ref. [15] for a brief overview. Meanwhile, as to the $(2 + 1)$ D $O(2)$ scalar field theory, which is relevant to the superfluid-Mott-insulator phase transition, the winding-angle- 2π -kink energy $\Delta E(2\pi)$, namely, vortex's energy, has been investigated under the outward-pointed [16] and C-periodic [17] boundary conditions with the Monte Carlo method. The former indicates that the critical amplitude ratio $\rho_s/\Delta E(2\pi)$ is indeed a universal constant in proximity to the critical point, whereas the latter revealed an infrared anomaly due

to kink's quantum undulations, claiming that the choice of the boundary condition exercises a subtle influence on kink's stability. In fairness, it has to be mentioned that in 3D, the character of the kink is arousing much attention away from the critical point [18, 19, 20, 21]. A comprehensive overview will be found in Ref. [22], where the *kinetic* energy cost of a vortex penetrating a finite-thickness plate is considered; in our simulation, the thickness is irrelevant, because the (2 + 1)D-*XY* criticality is concerned.

In the present paper, as a realization of the (2 + 1)D superfluid-Mott-insulator transition, we consider the 2D spin- $S = 1$ *XY* model. Here, the external field of a unit flux quantum ($\Phi = 2\pi$) is applied to the rectangular cluster uniformly by incorporating the phase factor $e^{i\phi_{ij}}$ (ϕ_{ij} : gauge angle between the i and j sites) into the hopping amplitudes. Taking the advantage in that the exact-diagonalization method allows us to treat such a complex-valued matrix element, we evaluated the excess energy cost $\Delta E(2\pi)$ due to $\Phi = 2\pi$ explicitly (without performing the inverse Laplace transformation). A key ingredient of our approach is that the finite-size-scaling behavior is improved by extending and adjusting the interaction parameters. Thereby, with the aid of the finite-size-scaling analysis, we show that the excess energy cost $\Delta E(2\pi)$ obeys the 3D-*XY* universality class, and the critical amplitude ratio $\rho_s/\Delta E(2\pi)$ takes a constant value in the *XY* phase.

As mentioned above, we consider the spin- $S = 1$ *XY* model instead of treating the soft-core boson model directly; namely, boson's creation and annihilation operators are regarded as quantum-spin's ladder operators [23, 24]. To be specific, the Hamiltonian for the $S = 1$ *XY* model is given by

$$\begin{aligned} \mathcal{H} = & -\frac{J_{NN}}{2} \sum_{\langle ij \rangle} (e^{i\phi_{ij}} S_i^+ S_j^- + e^{-i\phi_{ij}} S_i^- S_j^+) - \frac{J_{N NN}}{2} \sum_{\langle\langle ij \rangle\rangle} (e^{i\phi_{ij}} S_i^+ S_j^- + e^{-i\phi_{ij}} S_i^- S_j^+) \\ & + D \sum_{i=1}^N (S_i^z)^2 + D_{\square} \sum_{[ijkl]} (S_i^z + S_j^z + S_k^z + S_l^z)^2. \end{aligned} \quad (1)$$

Here, the quantum $S = 1$ spin \mathbf{S}_i is placed at each square-lattice point $i = 1, 2, \dots, N$. The position vector \mathbf{r}_i of each site i is given by the 2D Cartesian coordinates $\mathbf{r}_i = (x, y)$ with $x, y = 1, 2, \dots, L$ ($N = L^2$). The periodic (open) boundary condition is imposed along the x (y) direction. Hence, the $L \times L$ cluster forms the cylindrical surface, as shown in Fig. 1. In Eq. (1), the summations, $\sum_{\langle ij \rangle}$, $\sum_{\langle\langle ij \rangle\rangle}$, and $\sum_{[ijkl]}$, run over all possible nearest-neighbor, $\langle ij \rangle$, next-nearest-neighbor, $\langle\langle ij \rangle\rangle$, and plaquette, $[ijkl]$, spins, respectively. The parameters, J_{NN} , $J_{N NN}$, and D_{\square} , denote the respective coupling constants. The gauge twist angle ϕ_{ij} is mentioned afterward. The remaining parameter D stands for the single-ion anisotropy. Therefore, in the language of boson, the first two terms of the Hamiltonian (1) correspond to boson's kinetic energy, whereas the D and D_{\square} terms are the repulsive interactions among the on-site and intra-plaquette bosons, respectively. Therefore, the former (latter) enhances the superfluid (Mott insulator) phase.

The magnetic flux is applied by inserting a bar magnet into the cylinder; see Fig.

1. The gauge angle ϕ_{ij} is set to

$$\phi_{ij} = \int_{\mathbf{r}_i}^{\mathbf{r}_j} \mathbf{A}(\mathbf{r}) \cdot d\mathbf{r}. \quad (2)$$

Here, the vector potential $\mathbf{A}(x, y)$ is given by the expression

$$\mathbf{A}(x, y) = \left(\frac{y - \frac{1+L}{2}\Phi}{L(L-1)}, 0 \right), \quad (3)$$

(Landau gauge) with the flux Φ threatening the rectangular cluster as a whole. Hence, the unit-flux-quantum external field is realized by the setting $\Phi = 2\pi$.

As mentioned above, the interaction parameters $(J_{NN}, J_{NNN}, D, D_{\square})$ are optimized in order to improve the finite-size-scaling behavior. Namely, we survey the subspace

$$(J_{NN}, J_{NNN}, D, D_{\square}) = (jJ_{NN}^*, jJ_{NNN}^*, (2-j)D^*, D_{\square}^*), \quad (4)$$

parameterized by the variable j . Here, the optimal critical point [25]

$$(J_{NN}^*, J_{NNN}^*, D^*, D_{\square}^*) = (0.1582, 0.05856, 0.957, 0.1003) \quad (5)$$

was determined with the ordinary finite-size-scaling method combined with the real-space decimation so as to get rid of the irrelevant interaction terms [26], and attain suppressed corrections to scaling. The critical point j_c is thus given by

$$j_c = 1, \quad (6)$$

at which the set of parameters, $(J_{NN}, J_{NNN}, D, D_{\square})$, reduces to that of the critical point (5).

A schematic drawing of the ground-state phase diagram is shown in Fig. 2. For large $j > 1 (= j_c)$, the XY -ordered phase is realized, whereas in $j < 1$, the paramagnetic phase extends [27]. The criticality at $j_c = 1$ (6) belongs to the 3D- XY universality class [24]. In the language of boson, the XY (paramagnetic) phase corresponds to the superfluid (Mott insulator) phase [24]. As mentioned above, the gauge flux Φ (3) and the XY order conflict each other, and hence, the excess energy cost should take a non-zero value in the XY phase.

The rest of this paper is organized as follows. In Sec. 2, the simulation results for the XY model (1) are presented. Details of the finite-size scaling are explained as well. In Sec. 3, we present the the summary and discussions.

2. Numerical results

In this section we present the numerical results for the two-dimensional XY model (1) subjected to the gauge flux Φ (3). We employed the exact-diagonalization method, which enables us to treat the gauge-twisted complex-valued matrix element, and evaluate the excess energy cost due to $\Phi = 2\pi$ explicitly. In our preliminary survey, we found that irrespective of the value of Φ , the ground state belongs to the $(S_{tot}^z, k_x) = (0, 0)$ sector with the total longitudinal spin moment, S_{tot}^z , and x component of the wave vector, k_x . Within this subspace, the numerical diagonalization was performed. Hence,

the translational motion of the $\Phi = 2\pi$ kink is prohibited *a priori*, even though the translational drift costs very little energy with a quadratic (soft mode) dispersion relation, $\propto k_x^2$; it is an advantage of the exact-diagonalization method in that the quantum number k_x of kink's drift is under control.

2.1. Finite-size scaling of the excess energy cost $\Delta E(2\pi)$

In this section we consider the excess energy cost

$$\Delta E(2\pi) = E_0(2\pi) - E_0(0), \quad (7)$$

with the ground state energy $E_0(\Phi)$ of the Hamiltonian \mathcal{H} (1) under the gauge flux Φ (3). The gauge flux should create a winding-angle- Φ kink within the XY order.

In Fig. 3, we present the excess energy cost $\Delta E(2\pi)$ (7) for various values of the interaction parameter j (4) and the system sizes, (+) $L = 3$ (\times) 4, and (*) 5. The excess energy cost appears to develop in the XY phase, $j > j_c (= 1)$, whereas it vanishes in the paramagnetic phase, $j < j_c$. As anticipated, the excess energy cost reflects an elasticity of the XY order. Actually, this energy cost comes from the conflict between the superfluid state and the gauge flux reminiscent of the Meissner effect; the correspondence between the spin and boson pictures is shown in the chart, Fig. 2. Strictly speaking, unlike the Meissner effect, the flux takes a constant value irrespective of L , introducing a kink within the system. The texture of the kink is not pursued here, because such a snapshot picture is not available in the exact-diagonalization scheme.

We turn to the analysis of the criticality of the excess energy cost $\Delta E(2\pi)$. In Fig. 4, we present the scaling plot, $(j - j_c)L^{1/\nu} - \Delta E(2\pi)L$, of $\Delta E(2\pi)$ for various system sizes, (+) $L = 3$ (\times) 4, and (*) 5. The underlying idea behind the ordinate-axis scale, $\Delta E(2\pi)L$, is as follows. We made an assumption that $\Delta E(2\pi)$ should have the same scaling dimension as that of the mass gap m . Because the mass gap scales as the inverse correlation length $m \sim \xi^{-1}$ (along the imaginary-time direction), the expression $\Delta E(2\pi)L$ should be a scale-invariant quantity owing to the scaling hypothesis, $\xi \sim L$. On the one hand, the scale invariance of the abscissa scale, $(j - j_c)L^{1/\nu}$, follows immediately from the definition of the correlation-length critical exponent ν , *i.e.*, $\xi \sim |j - j_c|^{-\nu}$. The scaling parameters, j_c and ν , are set to $j_c = 1$ (6), and $\nu = 0.6717$ [28, 29], respectively. The latter is taken from the value of the 3D- XY universality class, as mentioned in Introduction. We stress that there is no *ad hoc* adjustable parameter undertaken in the present scaling analysis.

In Fig. 4, we see that the scaled $\Delta E(2\pi)$ data fall into the scaling curve satisfactorily, indicating that the quantity $\Delta E(2\pi)$ obeys the 3D- XY universality class. In other words, the simulation data for $\Delta E(2\pi)$ already enter into the scaling regime. Actually, owing to the fine tuning of the interaction parameters as in Eq. (4), corrections to scaling are eliminated [26] to a considerable extent. Encouraged by this finding, we further explore the criticality of the spin stiffness in the next section.

Last, we address a number of remarks. First, the scaling plot, Fig. 4, indicates that the winding-angle- $\Phi = 2\pi$ gauge field (3) indeed creates a point-like excitation, because

the excess energy cost $\Delta E(2\pi)$ has the same scaling dimension as the excitation mass, as confirmed above. In fact, away from the critical point $j \approx 1.5 (> j_c)$, in Fig. 3, kink's energy $\Delta E(2\pi)$ appears to be almost L -independent. Hence, kink's size should be sufficiently smaller than L , at least, away from j_c . Such a feature supports the mean-field (Bogoliubov-de Gennes) analysis [22], which states that kink's core is responsible for the kinetic mass. Last, in $(2 + 1)$ dimensions, the choice of the boundary condition is "problematical" [17] in regard to the vortex stability. In our setting, as depicted in Fig. 2, the system is translation invariant along the x axis, whereas the open boundary condition is imposed as to the y direction. In this sense, our setting is reminiscent of that of Ref. [16], where the outward-pointed boundary condition is imposed for all edges of the finite-size cluster, and vortex's mass is appreciated properly. Namely, the open boundary condition contributes to the stabilization of the vortex [17]. Moreover, the numerical diagonalization was performed within the zero-momentum ($k_x = 0$) subspace, and thus, the drift along the x direction is prohibited *a priori*. This treatment may also suppress the drift of the kink.

2.2. Finite-size scaling of the spin stiffness ρ_s

In this section we present the result for the spin stiffness ρ_s . For that purpose, in this section, the vector potential is set to the spatially uniform one

$$\mathbf{A}(\mathbf{r}) = \left(\frac{\theta}{L}, 0 \right), \quad (8)$$

with the gauge twist angle θ through the boundary condition along the x direction. This situation is realized by a sufficiently long bar magnet with the flux θ threatening through the cylinder. Clearly, this geometrical arrangement resembles that of Fig. 1. Accordingly, the gauge twist angle ϕ_{ij} in the Hamiltonian (1) has to be set in the same way as in Eq. (2). We are now able to impose the periodic boundary condition for both x and y directions, because the vector potential (8) is a constant one. Thereby, the spin stiffness was calculated as the elastic constant with respect to the distortion θ as

$$\rho_s = \left. \frac{\partial^2 E_0}{\partial \theta^2} \right|_{\theta=0}, \quad (9)$$

with the ground state energy E_0 of the Hamiltonian (1) under the gauge (8). In the XY phase, the spin stiffness should take a non-zero value because of the elasticity of the XY order.

To begin with, in Fig. 5, we present the spin stiffness ρ_s (9) for various values of the interaction parameter j and system sizes, (+) $L = 3$. (×) 4, and (*) 5. The spin stiffness develops in the XY phase, $j > j_c (= 1)$, whereas it is suppressed in the paramagnetic phase, $j < j_c$. Such a character resembles that of the excess energy cost $\Delta E(2\pi)$, and actually, the behaviors of Fig. 3 and 5 look alike. Hence, the spin stiffness should be a good counterpart of the excess energy cost, and the critical amplitude ratio between these quantities is investigated in the next section.

Aiming to examine the critical behavior of the spin stiffness, we present the scaling plot, $(j - j_c)L^{1/\nu} - \rho_s L$, for various system sizes, (+) $L = 3$, (\times) 4, and (*) 5, in Fig. 6. The underlying idea behind the scaling plot is as follows. The ordinate axis scale $\rho_s L$ is invariant in two spatial dimensions according to the scaling argument [1]; therefore, the spin stiffness has the same scaling dimension as that of the elementary excitation gap as well as $\Delta E(2\pi)$. On the one hand, the abscissa scale $(j - j_c)L^{1/\nu}$ is the same as that of Fig. 4. Additionally, the scaling parameters, j_c and ν , are the same as those of Fig. 4.

The scaling data in Fig. 6 overlap each other satisfactorily, confirming that the criticality is under the reign of the 3D-XY universality class. We stress that the scaling parameters, j_c and ν , are identical to those of Fig. 4. and there is no adjustable scaling parameters. Such a feature indicates that the optimized interaction parameters (4) indeed contribute to the suppression of corrections to scaling [26] even for ρ_s .

This is a good position to address a number of remarks. First, as demonstrated above, the spin stiffness (9) is less computationally demanding in the exact-diagonalization approach. With the world-line Monte Carlo method, the spin stiffness is evaluated systematically by the winding number of the world lines across the boundary condition [30]; this idea, however, does not apply to the Monte Carlo method based on the O(2)-scalar-field representation. Last, the spin stiffness ρ_s is not a mere theoretical concept, because it is observable experimentally [31, 32, 33]. Therefore, via ρ_s , other quantities can also be appreciated indirectly by relying on the critical amplitude ratios [3, 4, 5, 6, 7, 8, 9, 10, 11, 12, 13, 14]. In the next section, we follow this idea, choosing the excess energy cost $\Delta E(2\pi)$ as the denominator of critical amplitude ratio.

2.3. Critical amplitude ratio $\rho_s/\Delta E(2\pi)$

In this section, we turn to the analysis of the amplitude ratio $\rho_s/\Delta E(2\pi)$, following the preliminaries in Sec. 2.1 and 2.2.

In Fig. 7, we present the scaling plot, $(j - j_c)L^{1/\nu} - \rho_s/\Delta E(2\pi)$, of the amplitude ratio for various system sizes, (+) $L = 3$ (\times) 4, and (*) 5. Here, the scaling parameters, j_c and ν , are the same as those of Fig. 4. The ordinate axis $\rho_s/\Delta E(2\pi)$ is scaling invariant. Actually, in Sec. 2.1 and 2.2, it was found that the numerator and denominator, ρ_s and $\Delta E(2\pi)$, respectively, have the same scaling dimensionality, L^{-1} . The abscissa scale is the same as that of Fig. 4.

In Fig. 7, the scaled data overlap each other to form a plateau in the XY phase, $(j - j_c)L^{1/\nu} > 0$. Such a feature supports that the amplitude ratio $\rho_s/\Delta E(2\pi)$ indeed takes a universal constant in this domain. The plateau height is roughly estimated as $\rho_s/\Delta E(2\pi) \approx 0.5$ around $(j - j_c)L^{1/\nu} \approx 10$. Hence, for sufficiently large $L \rightarrow \infty$, this plateau regime j approaches toward the critical point as $j - j_c \rightarrow 0^+$. On the one hand, in the paramagnetic phase, $(j - j_c)L^{1/\nu} < 0$, a rapid convergence to $\rho_s/\Delta E(2\pi) \rightarrow 0$ is observed, while in close vicinity of the critical point, $(j - j_c)L^{1/\nu} \approx 0$, a steep development of a peak is seen. It would be reasonable that the ratio $\rho_x/\Delta E(2\pi)$ exhibits such singular

behaviors in the paramagnetic phase, where both numerator and denominator go to $\rho_s, \Delta E(2\pi) \rightarrow 0$ simultaneously, as $L \rightarrow \infty$.

In order to estimate the plateau height, namely, the amplitude ratio, precisely, in Fig. 8, we present the approximate amplitude ratio

$$(\rho_s/\Delta E(2\pi))^*(L) = \left. \frac{\rho_s}{\Delta E(2\pi)} \right|_{j=j_c^*(L)}, \quad (10)$$

for $1/L^2$. Here, the approximate critical point $j_c^*(L)$ denotes the extremal point

$$\left. \partial_j \frac{\rho_s}{\Delta E(2\pi)} \right|_{j=j_c^*(L)} = 0, \quad (11)$$

of the above-mentioned plateau for each L . The least-squares fit to the data in Fig. 8 yields an estimate $\rho_s/\Delta E(2\pi) = 0.539(7)$ in the thermodynamic limit, $L \rightarrow \infty$. In order to applicate a possible systematic error, replacing the abscissa scale of Fig. 8 with $1/L$, we carried out an alternative extrapolation analysis. Thereby, we arrived at a result, $\rho_s/\Delta E(2\pi) = 0.585(6)$. The deviation ≈ 0.05 from the aforementioned estimate 0.539 seems to dominate the least-squares-fitting error, ≈ 0.007 . Hence, regarding the former as the dominant source of uncertainty, we estimate the amplitude ratio as

$$\rho_s/\Delta E(2\pi) = 0.54(5). \quad (12)$$

We recollect a number of related studies. As mentioned in Introduction, according to the Monte Carlo simulation of the 3D classical O(2) scalar field theory under the outward-pointed boundary condition [16], the amplitude ratio was estimated as

$$\rho_s/\Delta E(2\pi) \approx 0.4. \quad (13)$$

This final result was obtained, relying on the preceding Monte Carlo data, $\rho_s/\Delta = 0.411(2)$ (Δ : Mott-insulator gap) [8]. This estimate (13) appears to lie out of the error margin of ours (12). As mentioned above, this result (13) was evaluated under the outward-pointed boundary condition [16]; see Fig. 9 (a). This boundary condition was implemented in such a way that rectangular-cluster-boundary spins are enforced to point outward, and thereby, an estimate, $\rho_s/m_V \approx 0.2$ (m_V : vortex mass) was obtained. This mass m_V corresponds to $m_V(= \Delta E(4\pi)) = 2\Delta E(2\pi)$, because of the winding-angle- $(\frac{2\pi}{4} \times 4)$ stress at each corner of the rectangular cluster and the winding-angle- 2π defect in the midst of the cluster. Hence, the aforementioned relation, $\rho_s/m_V \approx 0.2$ [16], admits an expression $\rho_s/\Delta E(2\pi) \approx 0.4$, Eq. (13), to adapt our notation. The discrepancy between the preceding result (13) and ours (12) might be attributed to the details of the boundary conditions undertaken. Actually, in our setting, Fig. 1, the periodic boundary condition is imposed on the x direction. On the contrary, the Monte Carlo simulation under the C-periodic boundary condition [17] (see Fig. 9 (b)) revealed an infrared anomaly for the vortex mass, claiming that the choice of the boundary condition leads to significant consequences as to this problem. Actually, according to this study [17], the vortex energy shows logarithmic divergences, as L increases. In our setting, on the contrary, kink's energy appears to be almost L -independent around

$j \approx 1.5$, as Fig. 3 indicates; namely, kink's stress energy concentrates in its core. That is, the periodic boundary condition promotes the infrared undulation of the kink. In our approach, the open boundary condition along the y axis [because of the Landau gauge (3)] and Hilbert-space's restriction within $k_x = 0$ are responsible for the stabilization of the kink, as argued in Sec. 2.1.

We address a number of remarks. First, the abscissa scale $1/L^2$ in Fig. 8 comes from the index $\omega_2 \approx 2$ [28] for next-to-leading scaling corrections. Because the leading ones are suppressed [25, 26] by adjusting the interaction parameters to Eq. (5), the universal quantity such as $\rho_s/\Delta E(2\pi)$ should obey the power-law behavior with this index $\omega_2 \approx 2$ for the small- L regime at least. Last, a peculiarity of the amplitude ratio $\rho_s/\Delta E(2\pi)$ is that in the opposite side (paramagnetic phase), the value is rather scattered; in contrast, Higgs-mass's amplitude ratio m_H/ρ_s , for instance, exhibits less singular behavior, and actually, it looks alike for both phases [12].

3. Summary and discussions

The excess energy cost $\Delta E(\Phi)$ (7) due to the external flux $\Phi = 2\pi$ in the superfluid phase was investigated by means of the exact-diagonalization method, with which one is able to treat the gauge-twisted complex-valued matrix elements. As a realization of the superfluid phase, we consider the quantum XY magnet (1) [24] with the extended interactions (4) to improve the finite-size-scaling behavior [26]. Actually, the excess energy cost $\Delta E(2\pi)$ appears to obey the 3D- XY universality class satisfactorily. Thereby, choosing the spin stiffness ρ_s as its counterpart, we analyzed the amplitude ratio, $\rho_s/\Delta E(2\pi)$, postulating that the criticality belongs to the 3D- XY universality class. The amplitude ratio $\rho_s/\Delta E(2\pi)$ exhibits a notable plateau around $(j - j_c)L^{1/\nu} \approx 10$, and thus, this plateau regime approaches to the critical point, $j - j_c \rightarrow 0^+$, as $L \rightarrow \infty$. The plateau height is estimated as $\rho_s/\Delta E(2\pi) = 0.54(5)$, Eq. (12). So far, under the outward-pointed [16] and C-periodic [17] boundary conditions, extensive simulations have been made. The former estimate $\rho_s/\Delta E(2\pi) \approx 0.4$, Eq. (13), appears to lie out of the error margin of ours, whereas the latter revealed an infrared anomaly, claiming that the choice of the boundary condition is significant. In the present study, the open boundary condition along the y axis and Hilbert-space's restriction within $k_x = 0$ contribute to the stabilization of $\Delta E(2\pi)$. Nevertheless, as demonstrated, the spin stiffness is of use to elucidate the universal character of $\Delta E(2\pi)$ quantitatively.

Through the duality transformation [34, 35, 36], the Mott-insulator state is interpreted as the condensed state of the vortices, and the vortex stiffness ρ_v now makes sense. Noticeably, this quantity ρ_v is accessible via the Nozières-Pines formula [37]. It would be tempting to evaluate the ratio $\rho_v/\Delta E(2\pi)$ across the Mott-insulator and superfluid phases as a “quantitative measure” [11] of deviation from self-duality. This problem is left for the future study.

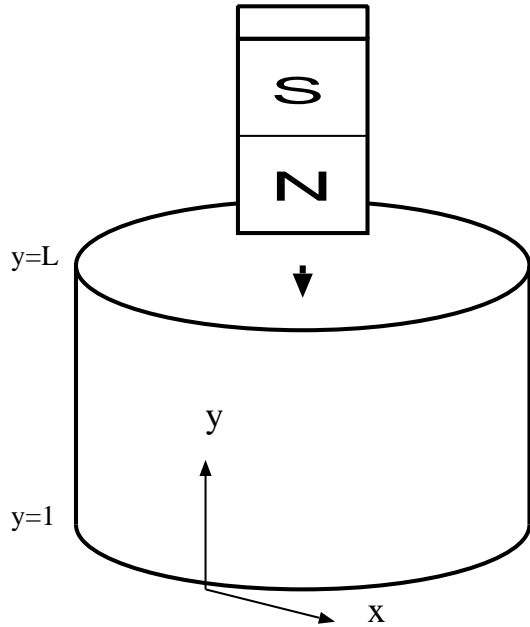


Figure 1. We consider the quantum XY model (1) on the rectangular cluster as a realization of the $(2 + 1)$ -dimensional superfluid-Mott-insulator transition [24]. We impose the periodic (open) boundary condition as to the x (y) direction, and hence, the rectangular cluster forms a cylindrical surface. Inserting the bar magnet into the cylinder, we apply the magnetic flux $\Phi = 2\pi$ per rectangular cluster perpendicular to the cylindrical surface a la Landau gauge (3).

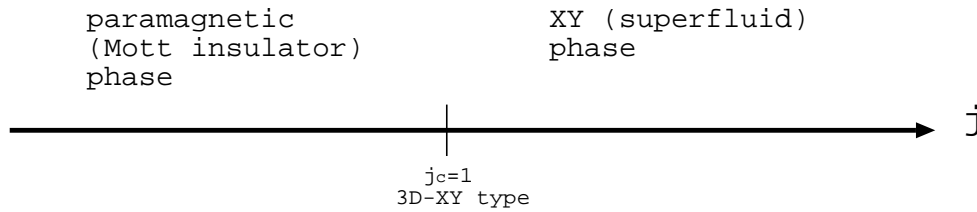


Figure 2. A schematic ground-state phase diagram for the two-dimensional XY model (1) with the coupling constants parameterized by j (4) is presented. For large (small) j , the XY (paramagnetic) phase is realized. In the boson language [24], each phase corresponds to the superfluid (Mott insulator) phase. The critical point at $j_c = 1$ (6) belongs to the 3D- XY universality class [27]. The scaling behavior is improved [26] by extending and adjusting the interaction parameters as in Eq. (4) [25].

Acknowledgments

This work was supported by a Grant-in-Aid for Scientific Research (C) from Japan Society for the Promotion of Science (Grant No. 20K03767).

- [1] M.P.A. Fisher, P.B. Weichman, G. Grinstein, and D.S. Fisher, Phys. Rev. B **40**, 546 (1989).
- [2] M. Swanson, Y. L. Loh, M. Randeria and N. Trivedi, Phys. Rev. X **4**, 021007 (2014).
- [3] F. Rose and N. Dupuis, Phys. Rev. B **95**, 014513 (2017).
- [4] F. Rose, F. Léonard, and N. Dupuis, Phys. Rev. B **91**, 224501 (2015).
- [5] A. Rançon, O. Kodio, N. Dupuis, and P. Lecheminant, Phys. Rev. E **88**, 012113 (2013).
- [6] A. Rançon and N. Dupuis, Phys. Rev. B **89**, 180501(R) (2014).

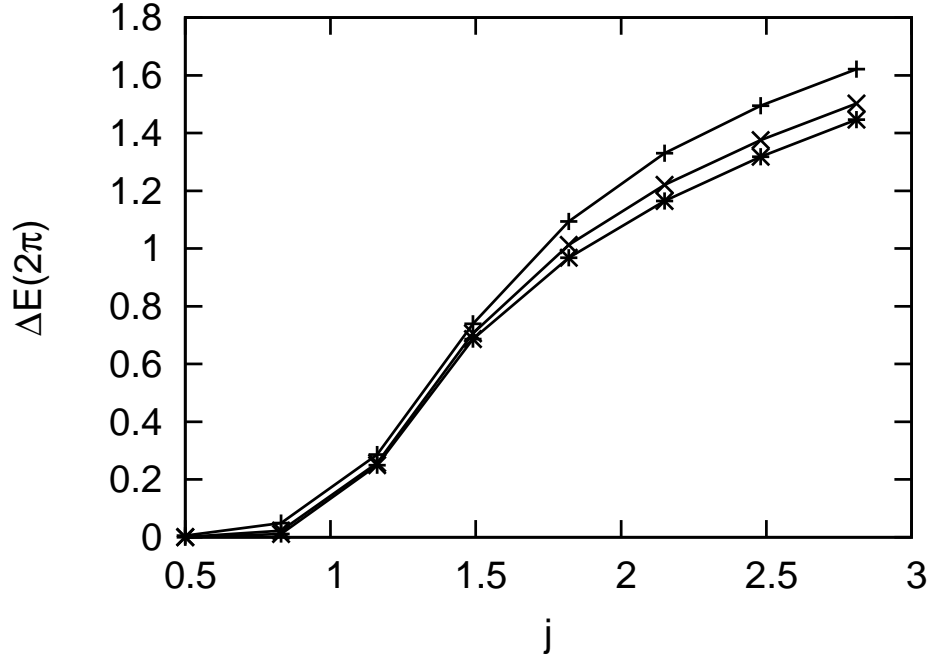


Figure 3. The excess energy cost $\Delta E(2\pi)$ (7) due to the gauge flux $\Phi = 2\pi$ is presented for the interaction parameter j (4) and the system sizes, (+) $L = 3$, (\times) 4, and (*) 5. In the XY (superfluid) phase $j > j_c (= 1)$, the excess energy cost $\Delta E(2\pi)$ develops.

- [7] Y. T. Katan and D. Podolsky, Phys. Rev. B **91**, 075132 (2015).
- [8] M. Hasenbusch, J. Stat. Mech. (2008) P12006.
- [9] S. Gazit, D. Podolsky, and A. Auerbach, Phys. Rev. Lett. **110**, 140401 (2013).
- [10] S. Gazit, D. Podolsky, A. Auerbach, and D. P. Arovas, Phys. Rev. B **88**, 235108 (2013).
- [11] S. Gazit, D. Podolsky, and A. Auerbach, Phys. Rev. Lett. **113**, 240601 (2014).
- [12] K. Chen, L. Liu, Y. Deng, L. Pollet, and N. Prokof'ev, Phys. Rev. Lett. **110**, 170403 (2013).
- [13] Y. Nishiyama, Nucl. Phys. B **897**, 555 (2015).
- [14] Y. Nishiyama, Eur. Phys. J. B **90**, 173 (2017).
- [15] N. Dupuis, L. Canet, A. Eichhorn, W. Metzner, J. M. Pawłowski, M. Tissier, and N. Wschebor, Phys. Rep. **910**, 1 (2021).
- [16] G. Delfino, W. Selke, and A. Squarcini, Phys. Rev. Lett. **122**, 050602 (2019).
- [17] M. Hornung, J. C. P. Barros, and U.-J. Wiese, arXiv:2106.16191.
- [18] J.-M. Duan, Phys. Rev. B **49**, 12381(R) (1994).
- [19] G. Baym and E. Chandler, J. Low Temperature Phys. **50**, 57 (1983).
- [20] N. B. Kopnin and M. M. Salomaa Phys. Rev. B **44**, 9667 (1991).
- [21] D. J. Thouless and J. R. Anglin, Phys. Rev. Lett. **99**, 105301 (2007).
- [22] T. Simula, Phys. Rev. A **97**, 023609 (2018).
- [23] T. Matsubara and H. Matsuda, Prog. Theor. Phys. **16** (1956) 569.
- [24] T. Roscilde and S. Haas, Phys. Rev. Lett. **99** (2007) 047205.
- [25] Y. Nishiyama, Phys. Rev. E **78**, 021135 (2008).
- [26] P. Hasenfratz, Prog. Theor. Phys. Suppl. **131**, 189 (1998).
- [27] H.-T. Wang and Y. Wang, Phys. Rev. B **71** (2005) 104429.
- [28] M. Campostrini, M. Hasenbusch, A. Pelissetto, and E. Vicari, Phys. Rev. B **74**, 144506 (2006).
- [29] E. Burovski, J. Machta, N. Prokof'ev, and B. Svistunov, Phys. Rev. B **74**, 132502 (2006).
- [30] E.L. Pollock and D.M. Ceperley, Phys. Rev. B **36**, 8343 (1987).

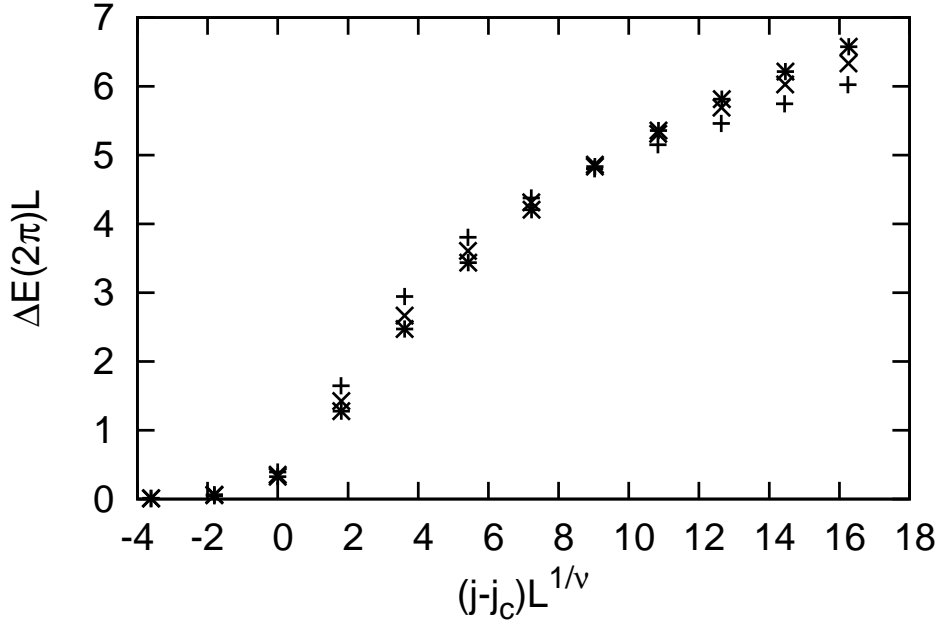


Figure 4. The scaling plot, $(j - j_c)L^{1/\nu} - \Delta E(2\pi)L$, of $\Delta E(2\pi)$ is shown for various system sizes, (+) $L = 3$, (\times) 4, and (*) 5. Here, the scaling parameters, namely, the critical point and correlation-length critical exponent, are set to $j_c = 1$ (6) and $\nu = 0.6717$ (3D-XY universality class) [28, 29], respectively. The simulation data collapse into the scaling curve satisfactorily, indicating that the simulation results already enter into the scaling regime. The scaling behavior appears to be improved [26] by the extension of the interaction parameters as in Eq. (4).

- [31] J. Corson, R. Mallozz, J. Orenstein, J. N. Eckstein and I. Bozovic, *Nature* **398**, 221 (1999).
- [32] R. W. Crane, N. P. Armitage, A. Johansson, G. Sambandamurthy, D. Shahar and G. Grüner, *Phys. Rev. B* **75**, 094506 (2007).
- [33] J. F. Sherson, C. Eitenberg, M. Endres, M. Cheneau, I. Bloch and S. Kuhr, *Nature* **467**, 68 (2010).
- [34] M. Stone and P.R. Thomas, *Phys. Rev. Lett.* **41**, 351 (1978).
- [35] M. P. A. Fisher and D. H. Lee, *Phys. Rev. B* **39**, 2756 (1989).
- [36] W.G. Wen and A. Zee, *Int. J. Mod. Phys. B* **04**, 437 (1990).
- [37] P. Nozières and D. Pines, *Nuovo Cim.* **9** (1958) 470.

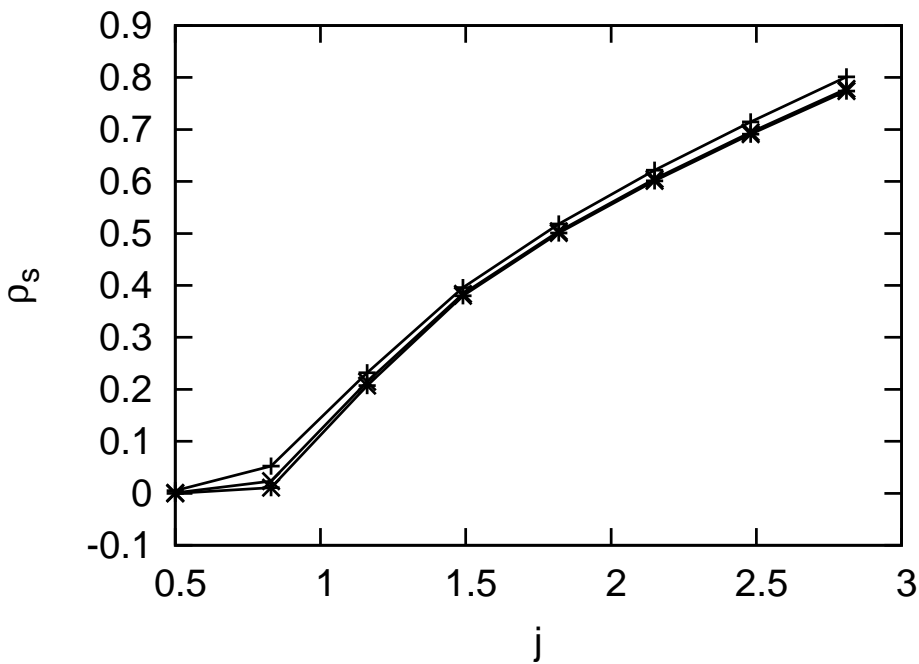


Figure 5. The spin stiffness ρ_s (9) is presented for the interaction parameter j (4) and various system sizes, (+) $L = 3$, (\times) 4, and ($*$) 5. In the XY (superfluid) phase $j > j_c (= 1)$, the spin stiffness develops in a way reminiscent of the excess energy cost $\Delta E(2\pi)$, as presented in Fig. 3.

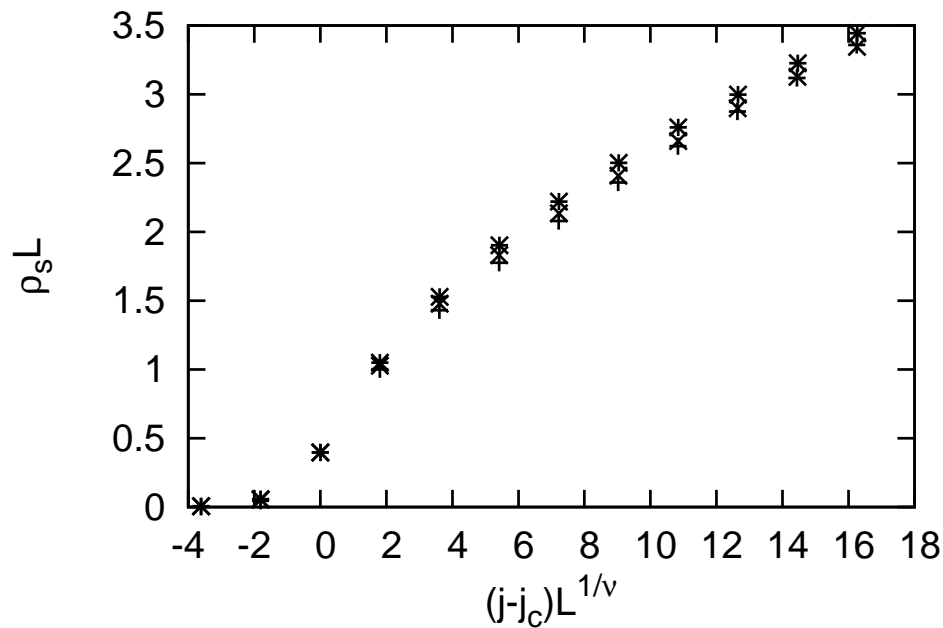


Figure 6. The scaling plot, $(j - j_c)L^{1/\nu} - \rho_s L$, of ρ_s is shown for various system sizes, (+) $L = 3$, (\times) 4, and (*) 5. Here, the scaling parameters, namely, the critical point j_c and the correlation-length critical exponent ν , are the same as those of Fig. 4. Even without any *ad hoc* adjustable parameters, the scaling data for ρ_s fall into the scaling curve satisfactorily, indicating that the criticality indeed belongs to the 3D-XY universality class.

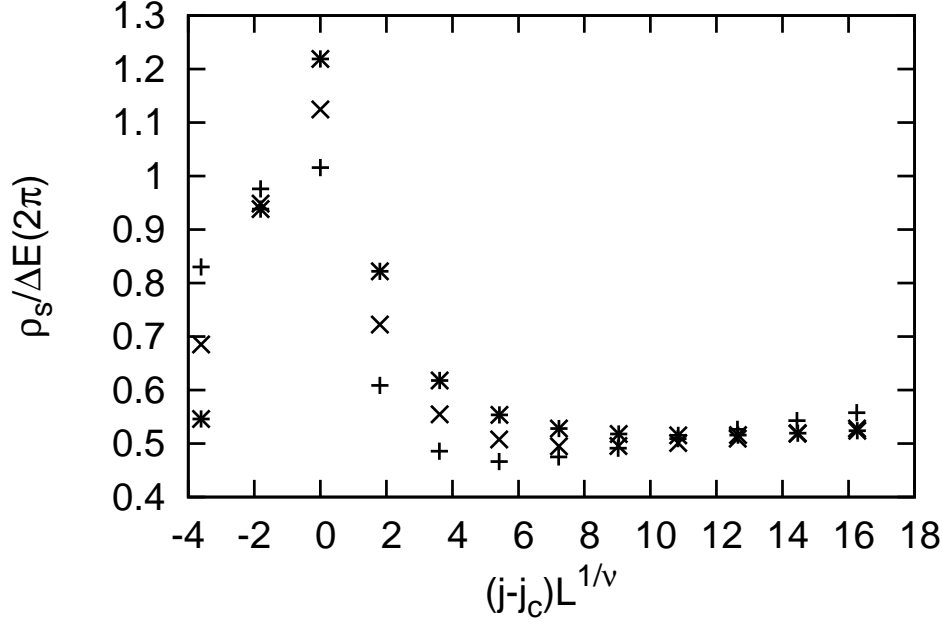


Figure 7. The scaling plot, $(j - j_c)L^{1/\nu} - \rho_s/\Delta E(2\pi)$, of the amplitude ratio is shown for various system sizes, (+) $L = 3$, (\times) 4, and ($*$) 5. Here, the scaling parameters, namely, the critical point j_c and the correlation-length critical exponent ν , are the same as those of Fig. 4. The amplitude ratio exhibits a notable plateau in the XY -phase side, $(j - j_c)L^{1/\nu} \approx 10$, indicating that the amplitude ratio takes a universal constant in proximity to the critical point.

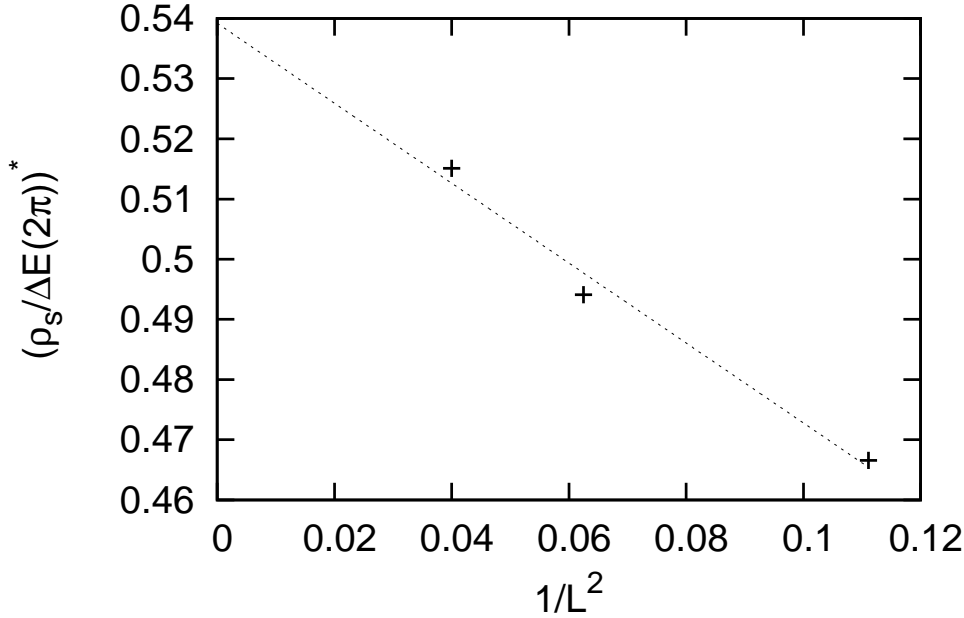


Figure 8. The approximate amplitude ratio $(\rho_s/\Delta E(2\pi))^*$ (10) is plotted for $1/L^2$. The least-squares fit to these data yields an estimate $\rho_s/\Delta E(2\pi) = 0.539(7)$ in the thermodynamic limit, $L \rightarrow \infty$. A possible systematic error is considered in the text.

Criticality of the excess energy cost due to the unit-flux-quantum external field for the (2+1)D superfluid-ins

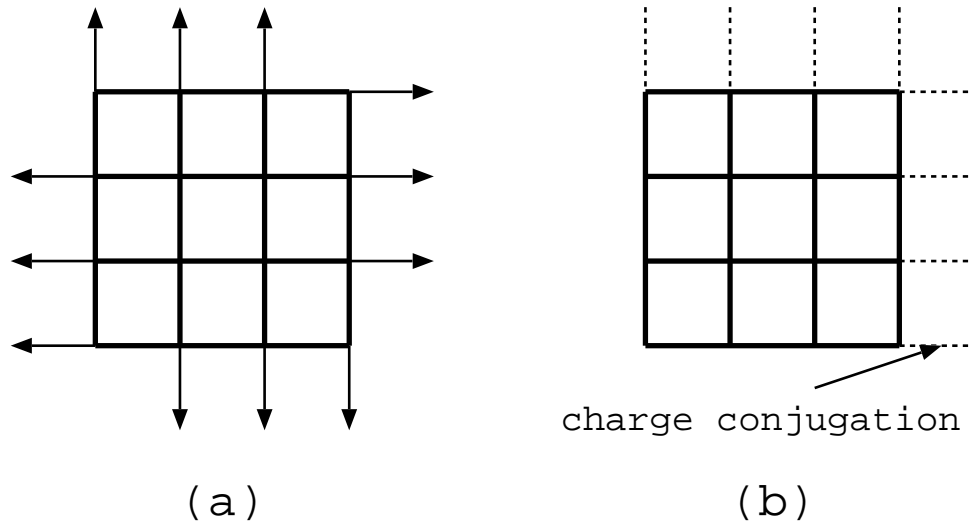


Figure 9. Schematic drawings for the (a) outward-pointed [16] and (b) C-periodic [17] boundary conditions are presented. In the former, the boundary spins are directed outward, whereas in the latter, there are imposed the periodic boundary conditions with the charge-conjugation twists, which “leave translation invariance intact” [17].